Supporting Information:

The Mechanism of Rectification in Tunneling Junctions Based on Molecules with Asymmetric Potential Drops

Christian A. Nijhuis, William F. Reus, and George M. Whitesides*

Department of Chemistry and Chemical Biology, Harvard University, 12 Oxford St, Cambridge, MA 02138, USA

corresponding author:

Tel.: 617 458 9430

Fax.: 617 458 9857

e-mail: gwhitesides@gmwgroup.harvard.edu

Nomenclature. We studied six different SAMs in this work: two SAMS of $SH(CH_2)_{11}Fc$ ($\equiv SC_{11}Fc$) and $SH(CH_2)_9Fc$ ($\equiv SC_9Fc$) with ferrocene (Fc) termini, a SAM of $SH(CH_2)_{11}Fc_2$ ($\equiv SC_{11}Fc_2$) with biferrocene (Fc_2) termini, a SAM of SAM $S(CH_2)_6Fc(CH_2)_5CH_3$ ($\equiv SC_6FcC_5CH_3$) with the Fc in the middle, and two SAMs of $SH(CH_2)_{10}CH_3$ ($\equiv SC_{10}CH_3$) and $SH(CH_2)_{14}CH_3$ ($\equiv SC_{14}CH_3$) with methyl termini. We use the general notation Ag^{TS}-$SC_{11}Fc$//Ga_2O_3/EGaIn to describe the junctions: here, Ag^{TS}-$SC_{11}Fc$ is a template-stripped silver thin-film electrode (with an area of about 1 cm^2) supporting a SAM of $SC_{11}Fc$. We describe the interfaces with the symbols "-", which

indicates a chemisorbed contact, "/" which indicates the interface between the Ga_2O_3 and bulk EGaIn, and "//", which indicates the presence of a non-covalent interface. The symbol *V* is defined as the difference in voltage between the two electrodes.

Experimental Details

Synthesis. The HSC_9Fc,[i] $HSC_{11}Fc$,[ii] and $SHC_{11}Fc_2$[iii] were prepared by previously reported methods.

$SC_6FcC_6CH_3$. We prepared the $Fc(CO)(CH_2)_5Br$ by a previously reported method.[i,ii] Friedels-Crafts of $Fc(CO)(CH_2)_5Br$ with $ClOC(CH_2)_4CH_3$ gave the $CH_3(CH_2)_5(CO)Fc(CO)(CH_2)_5CH_2Br$ following a previously reported procedure.[iv] ^1H NMR (500 MHz, $CDCl_3$) δ (ppm): 4.77 (t, 4H, J = 2 Hz, Fc), 4.48 (q, 4H, J = 2 Hz, Fc), 3.44 (t, 2H, J = 7 Hz, CH_2Br), 2.67 (t, 2H, J = 7 Hz, CH_2CO), 2.66 (t, 2H, J = 7 Hz) CH_2CO), 1.93 (p, 2H, J = 7 Hz, C**H**$_2CH_2Br$), 1.72 (m, 4H, C**H**$_2CH_2CO$), 1.51 (m, 2H, CH_2),1.35 (m, 4H, CH_2), 0.93 (t, 3H, J = 7 Hz, CH_3). Cald. for $C_{22}H_{29}BrFeO_2$ m/z = 461: found by ESI-MS: 461.1 $[M + H^+]$.

Clemmensen-reduction of $CH_3(CH_2)_5(CO)Fc(CO)(CH_2)_5CH_2Br$ gave $CH_3(CH_2)_5Fc(CH_2)_5CH_2Br$ following a procedure described by Creager et al.[ii] ^1H NMR (500 MHz, $CDCl_3$) δ (ppm): 4.77 (br, 8H, Fc), 3.40 (t, 2H, J = 7 Hz, CH_2Br), 2.30 (dt, 4H, J = 7 Hz, CH_2Fc), 1.86 (p, 2H, J = 7 Hz, C**H**$_2CH_2Br$), 1.45 (m, 6H, CH_2),1.33 (m, 8H, CH_2), 0.93 (*t*, 3H, J = 7 Hz, CH_3). Cald. for $C_{22}H_{33}BrFe$ m/z = 433, found by ESI-MS: m/z = 433.1 $[M + H^+]$.

Reaction of $CH_3(CH_2)_5Fc(CH_2)_5CH_2Br$ with thioeurea followed by basic hydrolysis gave $SC_6FcC_5CH_3$ following previously reported procedure.[ii] ^1H NMR (500 MHz, $CDCl_3$) δ

(ppm): 3.97 (t, 4H, J = 2 Hz, Fc), 3.96 (t, 4H, J = 2 Hz, Fc), 2.53 (q, 2H, J = 8 Hz, CH_2S), 2.31 (t, 2H, J = 7 Hz) CH_2Fc), 2.30 (t, 2H, J = 7 Hz) CH_2Fc), 1.64 (p, 2H, J = 7 Hz, C**H**$_2CH_2S$), 1.48 (m, 4H, CH_2),1.40 (m, 2H, CH_2), 1.30 (m, 8H, CH_2), 0.89 (*t*, 3H, J = 7 Hz, CH_3). ^{13}C NMR (125 MHz,$CDCl_3$) δ (ppm): 89.4 (Fc), 89.0 (Fc), 68.6 (Fc), 67.6 (Fc), 67.5 (Fc), 33.9, 31.7, 31.3, 31.1, 29.4, 29.3, 29.2, 28.9, 28.2, 24.5, 22.6, 14.1. Mass Cald. for $C_{22}H_{34}FeS$ m/z = 386, found by ESI-MS: m/z = 386.2 [M + H^+].

Purification $HSC_{10}CH_3$ and $HSC_{14}CH_3$. We purified the $HSC_{10}CH_3$ and $HSC_{14}CH_3$ (Aldrich) prior use by recrystallization from ethanol. The corresponding thiol was dissolved in ethanol at room temperature under an atmosphere of N_2. We filtered the solution after slowly cooling the solution to 0 ºC. The mother liquor was further cooled to -20 ºC overnight during which the crystals of the corresponding thiol formed. These crystals were collected by filtration. This procedure was repeated three times.

Formation of the SAMs. We immersed the Ag^{TS} surfaces within 5 s after removal from the wafer in the ethanolic solutions of the corresponding thiols (R.T., under argon) to minimize contamination of the metal surface. We formed the SAMs over 12 hours after which we rinsed the surfaces with ethanol to remove physisorbed materials.

Wet Electrochemistry. The SAMs of $SC_{11}Fc$, $SC_{11}Fc_2$, SC_9Fc, and $SC_6FcC_5CH_3$ were characterized at Au^{TS} electrodes by wet electrochemistry. Electrochemical measurements were performed with an AUTOLAB PGSTAT10. A custom built three-electrode setup equipped with a platinum counter electrode, a Ag/AgCl reference electrode, and a screw cap to hold the gold working electrode (area exposed to the solution = 0.44 cm^2) was used. Cyclic voltammograms were recorded in an aqueous solution 1 M $HClO_4$, between –0.1 and 0.9 V at scan rates of 0.050, 0.10, 0.20, 0.50, 1.0, 2.0 and 5.0 V/s.

Ag^{TS}-SAM//Ga_2O_3/EGaIn Tunneling Junctions. We formed ultra-flat Ag surfaces by a template-stripping (TS) procedure published previously.[v] Details can be found in reference v, but we give a brief description here. We deposited a layer of 500 nm of Ag by electron-beam (e-beam) evaporation at 2-3 × 10^{-6} Torr at a rate of 8-10 Å/s on silicon wafers with their native SiO_2 layer present. Glass slides (typically 1 cm^2 – cleaned by washing with EtOH, and subsequent exposure to oxygen plasma (500 Torr, 5min) – were glued at the Ag-surface using an optical adhesive (Norland, No. 61). We cured the optical adhesive by exposure to ultraviolet light for 2 h. The glass substrates were cleaved off the Si-wafer using a razor blade. After cleavage, we immersed the Ag^{TS} substrates in the ethanolic solutions containing the thiols under argon within 5 s to minimize contamination of the Ag^{TS} substrates.

Detailed descriptions of the procedures used to contact these SAMs by Ga_2O_3/EGaIn top-electrodes has been reported by our group.[vi] We used conical shaped eutectic indium-gallium (EGaIn, 75.5 % Ga 24.5 % by weight, 15.7 °C melting point) alloy as top-electrodes. The Ga_2O_3/EGaIn behaves as if it were a non-Newtonian fluid.[vii] When sheer-pressure is applied, Ga_2O_3/EGaIn behaves as a liquid. The Ga_2O_3/EGaIn will flow until the shear-pressure is relieved. This behavior allows Ga_2O_3/EGaIn, unlike mercury, to adopt non-spherical shapes. A drop of Ga_2O_3/EGaIn hanging from a 26S-guage needle was brought into contact with a surface that is wettable by Ga_2O_3/EGaIn (PDMS, glass, or Ag). The Ga_2O_3/EGaIn adheres to both the surface and to the needle. Slowly retracting the needle from the drop of Ga_2O_3/EGaIn-drop, using a micromanipulator, deformed the Ga_2O_3/EGaIn drop in such a way that two conically-shaped Ga_2O_3/EGaIn structures, connected head-to-head, formed. Further retraction of

the needle resulted in separation of the conically-shaped Ga_2O_3/EGaIn structures, one attached to the needle and the other attached to the surface. Subsequently, we discarded the substrate and replaced it by a Ag^{TS} surface with the SAM of interest, and contacted the SAM with the conically-shaped Ga_2O_3/EGaIn at the needle.

Wet Electrochemistry. The shape of the cyclic voltammagrams gives qualitative information about the types of defects, structure, and quality of the SAMs. Strongly interacting redox centers result in peak broadening, and shifts the $E_{1/2}$ to more positive potentials.[viii,ix] For the SAMs of SC_9Fc, $SC_{11}Fc$, and $SC_{11}Fc_2$ we observe this peak broadening; it indicates that the Fc moieties do interact with each other and are confined in the top of the SAM. For the SAMs of SC_9Fc, however, we observe a shoulder at ~430 mV. We do not observe this shoulder, or it is perhaps too small to be observed, for SAMs of $SC_{11}Fc$ and $SC_{11}Fc_2$. This shoulder might be caused by Fc moieties that folded back in the SAM and point to the Au^{TS} electrode rather than to the electrolyte solution.[x]

The cyclic voltammograms of the SAMs of $SC_6FcC_5CH_3$ show more complex behavior. A SAM that was formed over 12 h had a $E_{1/2}$ of 0.521 ± 0.007 SAM and wider oxidation waves (Figs. S1D and S1E), while those formed over 30 s had a $E_{1/2}$ of 462 ± 2 mV and narrower oxidation waves (Fig. S1F). These observations indicate that the SAMs formed over 12 h have more strongly interacting Fc moieties, and are more ordered than those formed over 30 s. The SAMs that were formed over 12 h showed an additional wave at $E_{1/2}$ = 0.33 ± 0.03 V which had a ten times smaller surface area than the main

Figure S1: Cyclic voltammograms of the redox-active SAMs on Au^{TS} electrodes. The SAMs were formed for 24 h using a 2-3 mM ethanolic solutions of the corresponding thiols at R.T. under an argon atmosphere. The cyclic voltammograms where recorede using aqueous 1 M $HClO_4$ as electrolyte solution, and the potentials are vs. Ag/AgCl; The cyclic voltammograms of A) $SC_{11}Fc$ at scan rate = 2.0, 1.0, 0.50, 0.20, 0.10, and 0.050 V/s; B) SC_9Fc at scan rate = 2.0, 1.0, 0.50, 0.20, 0.10, 0.050, 0.020, and 0.010 V/s; C) $SC_{11}Fc_2$ at scan rate = 2.0, 1.0, 0.50, 0.20, 0.10, 0.050, 0.020, and 0.010 V/s; D) $SC_6FcC_5CH_3$ at scan rate = 2.0, 1.0, 0.50, and 0.20 V/s; E) $SC_6FcC_5CH_3$ at scan rate = 0.10, 0.050, 0.020, and 0.010 V/s; and F) $SC_6FcC_5CH_3$ at scan rate 2.0, 1.0, 0.50, 0.20, 0.10, 0.050, 0.020, and 0.010 V/s of SAM that was formed over 30 s.

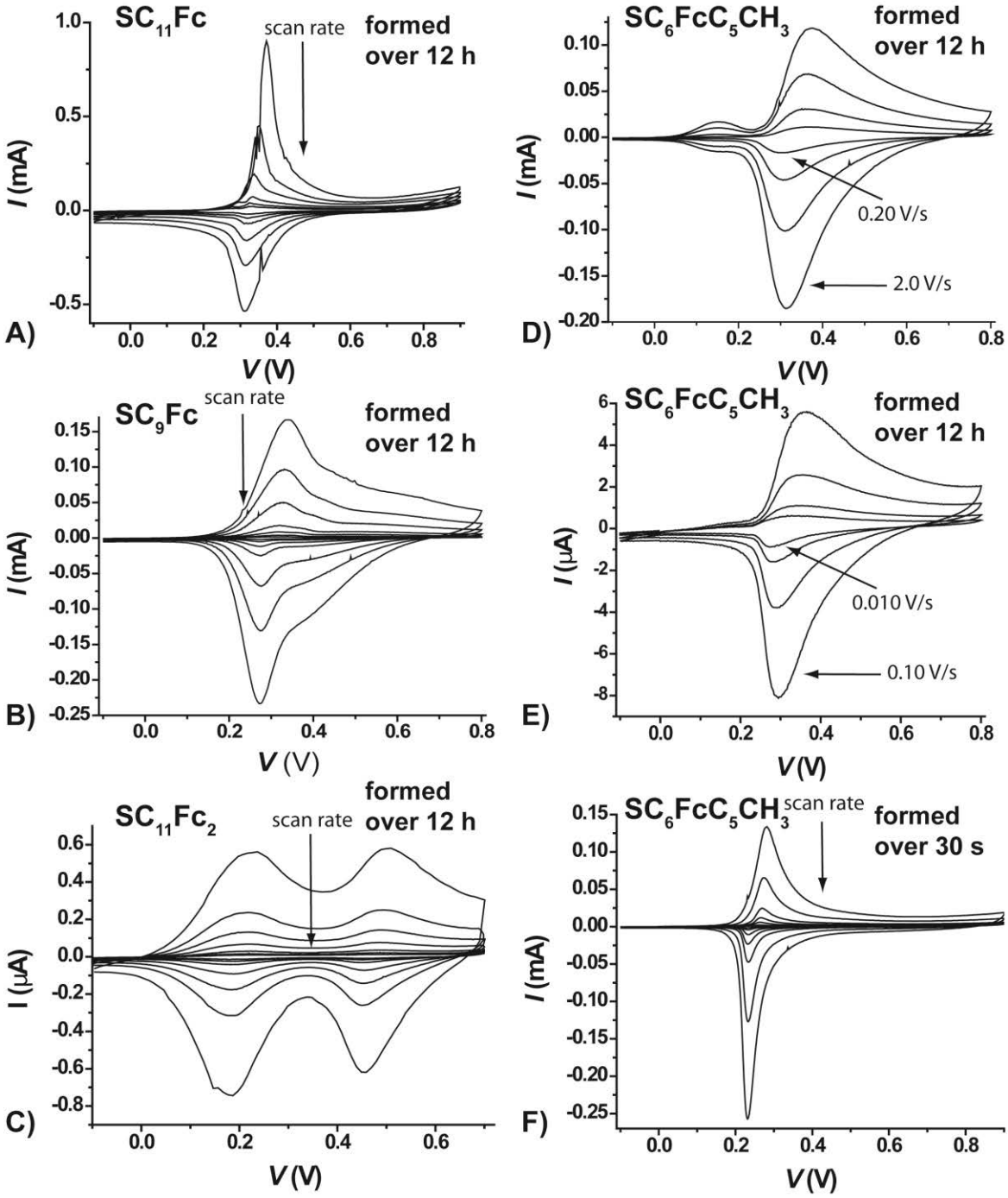
A)
SC11Fc
scan rate
formed over 12 h
I (mA)
V (V)
B)
SC9Fc
scan rate
formed over 12 h
I (mA)
V (V)
C)
SC11Fc2
scan rate
formed over 12 h
I (μA)
V (V)
D)
SC6FcC5CH3
formed over 12 h
0.20 V/s
2.0 V/s
I (mA)
V (V)
E)
SC6FcC5CH3
formed over 12 h
0.010 V/s
0.10 V/s
I (μA)
V (V)
F)
SC6FcC5CH3
scan rate
formed over 30 s
I (mA)
V (V)

peak. This wave disappeared with low scan rates $\upsilon \leq 0.1$ V/s, and was only visible at high scan rates $\upsilon \geq 0.2$ V/s (Figs. S1D and S1E). This redox wave might originate from Fc moieties that are in close proximity, or even in contact, with the Au^{TS} bottom-electrode, but shielded from the electrolyte solution by the rest of the SAM. It has been reported that strongly physisorbed redox-active species on the electrodes can have lower shift the values of $E_{1/2}$ to more negative values than those that do not interact strongly with the electrode.[Error! Bookmark not defined.] We did not observe this second oxidation wave for SAMs with short times of formation (30 s) which indicate that the SAM had no Fc moieties interacting with the Au^{TS} bottom-electrode (neither did all other SAMs surveyed in this study). We believe that the SAMs formed over 30 s have most of the Fc moieties separated from the Au^{TS} bottom-electrode by the C_6 alkyl chain, but the second C_6 alkyl chain might be highly disordered and fold back in the SAM and point toward the gold surface (the surface coverages of both types of SAMs were similar (>95% forms during the first second, but ordering of the SAMs is a much slower process**Error! Bookmark not defined.**). The Fc moieties in the SAMs formed over 12 h have the second alkyl chain pointing away from the Au^{TS} bottom-electrode – pointing to the electrolyte solution – which agrees with the shift of the $E_{1/2}$ to more positive potentials (by 60 mV).[Error! Bookmark not defined.] Chidsey et al. reported that SAMs in which the Fc moieties are shielded from the electrolyte solution by alkyl chains have peak oxidation potentials shifted to more positive values.[xi] The fact that at low scan rates this wave at lower positive potentials is not observed may indicate that the interaction of the Fc moieties with bottom-electrode is weak. Thus, we believe that most of the Fc moieties are separated from the Au^{TS} bottom-electrode by the C_6 moiety, but some (~10%) Fc moieties might

form direct, weak contact with the Au^{TS} bottom-electrode at sites with defects. Thus, most Fc moieties are roughly located in the middle of the SAM.

Statistical Analysis of the Junctions. A typical statistical analysis is described here for junctions with SAMs of $SC_{11}Fc$, but similar analyses were performed for the junctions with the five other types of SAMs (See Table 3). In total, we recorded 997 J(V) traces (1 trace = 0V → +1V → -1V → 0V) from 53 Ag^{TS}-$SC_{11}Fc$//Ga_2O_3/EGaIn junctions assembled on ten different Ag^{TS} substrates (five to six junctions per substrate). The Ag^{TS} substrates on glass were obtained from three different Ag coated wafers. Of the 53 junctions examined, three junctions (5%) failed on the first trace: that is, they showed either no electrical contact or a short circuit. During subsequent measurement two junctions suffered from excessive noise, one from a loss of contact, and one from a short-circuit (defined as a sudden increase in current density of more than two orders of magnitude). The remaining 46 junctions continued to rectify for 21 traces, after which the experiment was terminated so that every junction would weigh equally in the statistical analysis. Thus, the yield of stable junctions is 87% and the number of traces recorded on the junctions is 997, from which the $\langle \log|J| \rangle$ values and R were determined.

We used a nonlinear least-squares fitting algorithm (the curve-fitting tool in MATLAB R2007a)[xii] to fit Gaussians to the histograms of current densities and rectification ratios. Since R and J were log-normally distributed, the normally-distributed variables log(R) and log(J) served as the input to the fitting algorithm, so that the algorithm always fit Gaussians to normally-distributed data.[xii] The mean (μ) and standard

deviation (σ) extracted from each Gaussian fit were transformed to the log-mean (μ_{log}) and log-standard deviation (σ_{log}) according to the formulae: $\mu_{log} = 10^{\mu}$ and $\sigma_{log} = 10^{\sigma}$.

We stress that every measurement, without exception, collected for each type of junction was included in both the corresponding histogram and the input to the fitting algorithm that determined the Gaussian fit. Thus, in plotting and fitting the data, we neither excluded nor omitted any value. In some figures, the Gaussian fit appears not to conform to a region of the histogram, as if the data in that region had been excluded from the fitting process; however, no data were excluded. Though a particular Gaussian fit may be visually unsatisfying, all fits are reproducible because they result from the minimization of error by the fitting algorithm without interference from the operator. We believe that the community should adopt this approach – or another similarly straightforward and unbiased strategy – concerning the presentation and fitting of data.

Electrical Properties of the Layer of Ga_2O_3. We have measured the resistance of the layer of Ga_2O_3 in two ways. First, as reported previously,[xiii] we made a grazing contact to the Ga_2O_3 using a thin (~ 80 μm diameter) copper wire and grounded the bulk EGaIn using another copper wire penetrating the layer of Ga_2O_3. Current flowing through this circuit met a resistance that was a factor of ~ 65 greater than that of two copper wires contacting bulk EGaIn, so the layer of Ga_2O_3 does offer some electrical resistance. However, the resistance density (resistance multiplied by contact area) of the contact between the copper wire and the layer of Ga_2O_3 was 0.04 Ω-cm^2, which is three orders of magnitude less than the resistance density (50 Ω-cm^2) of a junction containing a SAM of SC_9CH_3 (the most conductive SAM we measure).

Second, we contacted cone-shaped tips of Ga_2O_3/EGaIn to transparent electrodes of ITO (tin-doped indium oxide) while measuring the current in real time at an applied bias of 50 mV. We recorded optical micrographs through the transparent ITO to determine the size of the junctions. Figure S2 shows that the current increased (as expected) with the junction size, but suddenly increased by a factor of about ~100 at t = 340 s. This value of the current is similar to that of a circuit without the cone-shaped tip of Ga_2O_3/EGaIn, i.e., ITO contacted directly with a metal probe biased at 50 mV.

We believe that this sudden increase in the current results from the formation of direct contact of bulk EGaIn with the ITO. The resistance density of this particular circuit was 0.4 Ω-cm^2, still two orders of magnitude less than that of the most conductive SAM we measure. In our junctions, therefore, current through the circuit is limited by the SAM, not by the layer of Ga_2O_3.

By estimating the area of contact between Ga_2O_3 and ITO from the optical micrographs in Figure S1 and assuming that the thickness of the layer of Ga_2O_3 is 2 nm, we calculated a resistivity of $\rho = \sim 10^6$ Ω-cm for the Ga_2O_3. Paterson et al.[xiv] reported a resistivity of $\rho = \sim 10^{10}$ Ω-cm in the low-bias regime (0 V < V < 0.4 V) for a 10 nm-thick film of epitaxially grown Ga_2O_3 on GaAs. Since the native film of Ga_2O_3 on EGaIn forms spontaneously in air, it likely contains many more defects and is thus more conductive than an epitaxially grown film.

In order to establish the mechanism of charge-transport in Ga_2O_3, we contacted the layer of Ga_2O_3 on a drop of EGaIn using Cu wires, as described above, and performed measurements of charge-transport at various temperatures (Figure S3). Starting at 295 K, we incrementally decreased the temperature while measuring current vs. applied bias. At

Figure S2: The current measured as a function of time while contacting a cone-shaped tip of Ga_2O_3/EGaIn to ITO. At t = 5 s the tip contacted the ITO and allowed a current of 3.2 μA to flow. The current increased as the junction size increased (optical micrographs show the footprint of the junction, seen from below the ITO, at various times) until, at *t* = 340 s, the current suddenly increased to ~200 μA.

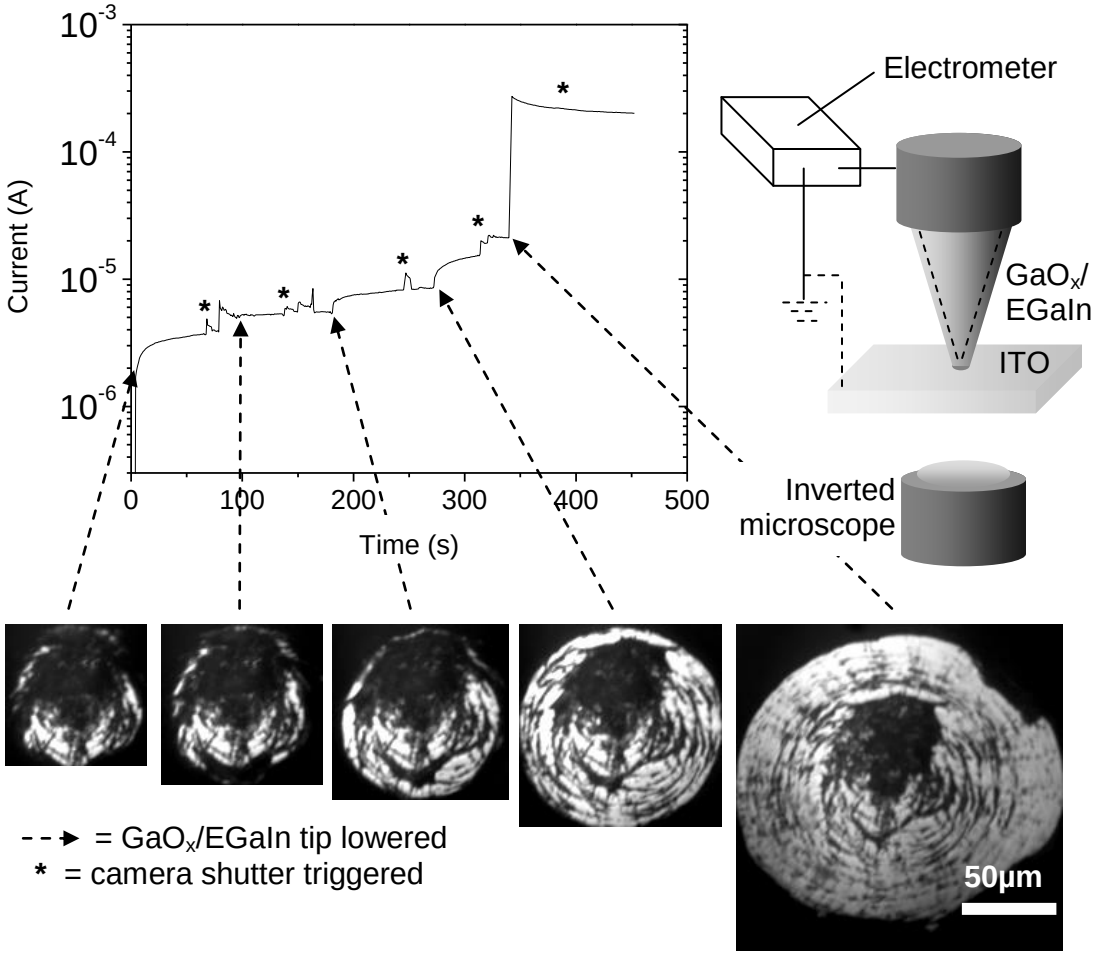
Current (A)
10-3
10-4
10-5
10-6
0
100
200
300
400
500
Time (s)
Electrometer
GaOx/
EGaIn
ITO
Inverted
microscope
= GaOx/EGaIn tip lowered
* = camera shutter triggered
50μm

260 K, the liquid EGaIn solidified, disturbing the contact between Cu and Ga_2O_3 and hindering further measurements.

However, in the range of 295 – 260 K, we observed a strong dependence of current on temperature, indicating that charge-transport proceeds *via* a thermally activated process. We plan to report a detailed analysis of these results in a separate paper;[xv] however, our observation of thermally activated charge-transport agrees with Paterson et al.,[xiv] who reported that thermionic emission was the dominant mechanism of charge-transport through epitaxially grown films of Ga_2O_3 on GaAs.

Figure S3: Current vs. applied bias at four temperatures in the range 295 K – 260 K for a Cu wire contacting the layer of Ga_2O_3 on the surface of a drop of EGaIn.

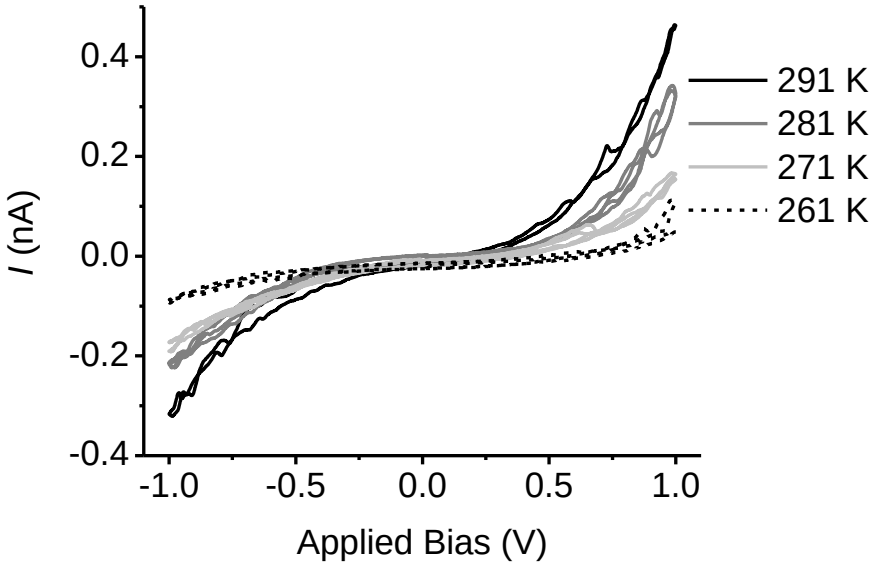
0.4
0.2
0.0
-0.2
-0.4
I (nA)
-1.0
-0.5
0.0
0.5
1.0
Applied Bias (V)
291 K
281 K
271 K
261 K

Figure S4: An example of Ag^{TS}-$SC_{11}Fc_2$//Ga_2O_3/EGaIn junction that was stable during *J*(V) measurement of ± 2.0 V. This figure shows 9 *J*(V) traces after which we terminated the experiment.

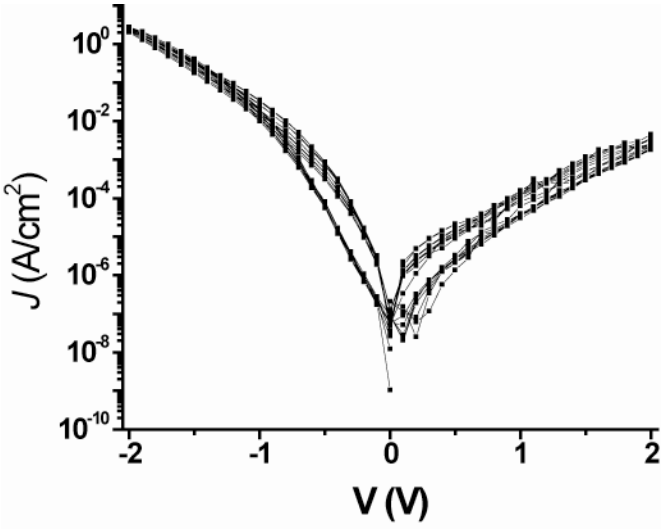
10^{0}
10^{-2}
10^{-4}
10^{-6}
10^{-8}
10^{-10}
J (A/cm^2)
-2
-1
0
1
2
V (V)

References

[i] Sumner, J. J.; Weber, K. S.; Hockett, L. A.; Creager, S. E. *J. Phys. Chem. B* **2000**, *104*, 7449.

[ii] Creager, S. E.; Rowe, G. K. *J. Electroanal. Chem.* **1994**, *370*, 203.

[iii] Dong,T. -Y.; Chang, L. -S.; Tseng, I. -M.; Huang, S. -J. *Langmuir*, **2004**, *20*, 4471.

[iv] Han, S. W.; Seo, H. Y.; Chung, K.; Kim, K. *Langmuir* **2000,** *16,* 9493

[v] Weiss, E. A.; Chiechi, R. C.; Kaufman, G. K.; Kriebel, J. K.; Li, Z.; Duati, M.; Rampi, M. A.; Whitesides G. M. *J. Am. Chem. Soc.* **2007**, *129*, 4336.

[vi] Chiechi, R. C.; Weiss, E. A.; Dickey, M. D.; Whitesides, G. M. *Angew. Chem. Int. Ed.* **2008**, *47*, 142.

[vii] Dickey, M. D.; Chiechi, R. C.; Larson, R. J.; Weiss, E. A.; Weitz, D. A.; Whitesides, G. M. *Adv. Funct. Mater.* **2008**, *18*, 1097.

[viii] Chidsey, C. E. D.; Bertozzi, C. R.; Putvinski, T. M.; Mujsce, A. M. *J. Am. Chem. Soc.* **1991**, *112*, 4301.

[ix] Weber, K.; Hockett, L.; Creager, S. *J. Phys. Chem. B* **1997**, *101*, 8286.

[x] Auletta, T.; van Veggel, F. J. C. M; Reinhoudt, D. N. *Langmuir* **2002**, *18*, 1288.

[xi] Rowe, G. K.; Greager, S. E. *Langmuir* **1991**, *7*, 2307.

[xii] We obtained Gaussian fits using a least-squares, trust-region based algorithm: the 'gauss1' model (all options set to default) in the curve-fitting toolbox in MATLAB 7.4.0.287 (R2007a) Copyright The MathWorks, Inc. 1984-2007. No weighting or exclusion rules were applied to the data.

[xiii] Nijhuis, C. A; Reus, W. F.; Whitesides, G. M. *J. Am. Chem. Soc.* **2009**, *131*, 17814.

[xiv] Paterson, G. W.; Wilson, J. A.; Moran, D.; Hill, R.; Long, A. R.; Thayne, I.; Passlack, M.; Droopad, R. *Mater. Sci. Eng. B*, **2006**, *135*, 277.

[xv] Reus, W. F.; Nijhuis, C. A.; Barber, J.; Mwangi, M.; Cademartiri, L.; Kim, C.; York, R. L.; Liu, X.; Whitesides, G. M. unpublished results.